Eur. Phys. J. D **1**, 85–91 (1998)

**THE EUROPEAN PHYSICAL JOURNAL D**



# Electromagnetically induced transparency in a RF discharge

F.S. Pavone[1], M. Artoni[1], G. Bianchini[1], P. Cancio[2], F.S. Cataliotti[3], and M. Inguscio[3,a]

[1] European Laboratory for Nonlinear Spectroscopy (LENS) Istituto Nazionale di Fisica della Materia (INFM) L.go E. Fermi 2, 50125, Firenze, Italia
[2] C.S.I.C., Instituto de Estructura de la Materia, Serrano 123, 28006 Madrid, Spain
[3] Dept. of Physics University of Firenze, Firenze, Italia

Received: 1 August 1997 / Accepted: 13 October 1997

**Abstract.** We report on electromagnetically induced transparency in a radio-frequency discharge of metastable helium atoms. We show that a large effect can be observed in spite of the discharge regime needed to produce the metastable helium and in spite of its Zeeman degeneracy. We discuss the mechanism and the conditions for the observation of such a phenomenon in a helium discharge.

**PACS.** 42.50.Gy Effects of atomic coherence on propagation, absorption, and amplification of light – 32.80.-t Photon interactions with atoms – 52.25.Rv Emission, absorption, and scattering of visible and infrared radiation

Quantum coherence in a multi-level system has led to the observation of many interesting phenomena. In particular, it is possible to make an optically opaque transition transparent to a weak probe beam when a strong laser is tuned onto resonance with another transition that shares a common level with the opaque one [1]. The coherence induced by the strong beam is such that the dipole moment at the probe field becomes so small that atom and probe are nearly decoupled. This effect, where one field controls the complex refractive index of the other, is called electromagnetically induced transparency and it is now reasonably well understood in all three-level atomic configurations. To some extent such a transparency is of long standing: it already appears as a special case in the work of Lambropoulos [2], Rzazewski [3], Ravi [4] and it is also much similar in nature to that observed by Whitley [5] and Alzetta [6] in the Rayleigh scattering of radiatively broadened systems. Electromagnetically induced transparency, however, has recently attracted much attention and there exists an extended literature on the subject either on its own right or on its relation to gain [7] and lasing [8] without inversion, to non-linear optics [9] and trapping of cold atoms (dark states) [10]. Such an effect can be used, *e.g.*, to control the complex refractive index [11], to produce transparency in the continuum [12], to eliminate self-focusing [13], to induce atomic birefringence [14], and to enhance isotope discrimination [15].

In the present work we extend the observation of electromagnetically induced transparency to a radio-frequency discharge of metastable $^4$He. The experimental demonstration of this effect is mainly complicated by the Zeeman level degeneracy of helium. Similar and somehow more conspicuous difficulties exist for the case of alkali atoms because of their complex hyperfine level structure. Further complications arise in our case from the discharge process used to produce metastable atomic helium; collisional processes (ion-atom, electron-atom, *etc.*) can easily degrade the coherence between atomic levels. In the present work we recover most features common to induced transparency found in previous experiments [16] and we further anticipate new characteristics specific to the realization of such an effect in a radio- frequency discharge regime. The dependence, *e.g.*, of the transparency on the gas pressure and polarizations of the laser beams is thoroughly investigated. We will see that in our specific system optimal induced transparency is realized when the intensity of the coupling laser (*cf.* Fig. 1a) becomes appreciably larger than the saturation intensity of the corresponding transition times the ratio of the characteristic level broadenings.

In our experiment we probe the transmission of a weak laser beam tuned near a $2S_1 \leftrightarrow 2P_j$ transition (Fig. 1b) with, and without, a strong coupling beam tuned to the relevant $2P_J \leftrightarrow 3S_1$ transition. Metastable helium is produced by a radio-frequency discharge in a cell; the strong beam (706 nm) originates from a Ti:Sa ring laser while the weak probe radiation is provided by a DBR semiconductor diode laser (1083 nm). The counter propagating probe and coupling beams can have circular polarizations or linear polarizations, whose relative orientation can be varied, and are focused into the center of the cell with beam diameters of 100 $\mu$m and 140 $\mu$m , respectively. The probe beam is centered on the spatially uniform central portion

[a] e-mail: laserspec@fi.infn.it

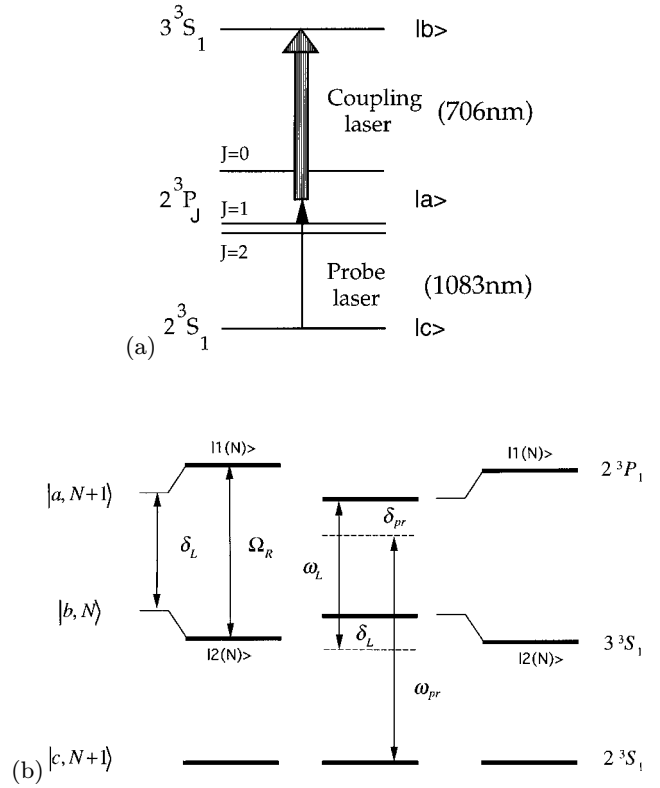


**Fig. 1.** (a) Atomic transitions and states used in the experimental demonstration of electromagnetically induced transparency in a $^4$He radio-frequency discharge. (b) The probe and coupling laser beams are tuned onto the $2S_1 \leftrightarrow 2P_1$ and $2P_1 \leftrightarrow 3S_1$ transitions, respectively. The strong coupling beam AC-Stark splits the levels ($\delta_{\rm L} > 0$) which become separated by an amount $\Omega_{\rm R}$. The probe sees dressed states $|\,1(N)\rangle$ and $|\,2(N)\rangle$ which are linear combinations of the uncoupled states $|\,{\rm a},\ N+1\rangle$ and $|\,{\rm b},\ N\rangle$.

of the larger coupling beam and remain centered over the length of the cell. High power values of the coupling laser are realized by means of an external build-up cavity frequency locked to the laser. A scheme of the experimental apparatus is shown in Figure 2.

We start by presenting an interesting aspect of the observed electromagnetically induced transparency in metastable helium. In the absence of the coupling laser the probe is absorbed while in its presence various degrees of probe transparency are observed to depend on the angle between the polarization of the coupling and probe lasers. With the coupling laser on, one expect single photon-absorption as well as two-photon absorption processes to occur. This expectation is correct when the detuning $\delta_{\rm L}$ of the coupling laser is significantly larger than its Rabi frequency $\Omega_L$. However, the system is expected to exhibit a rather different behavior when the Rabi frequency of the coupling laser is larger than the detuning or than the linewidth of the transitions involved (vanishing detuning). In our experiment the probe and coupling beams are taken to be resonant onto the $2S_1 \leftrightarrow 2P_1$ and

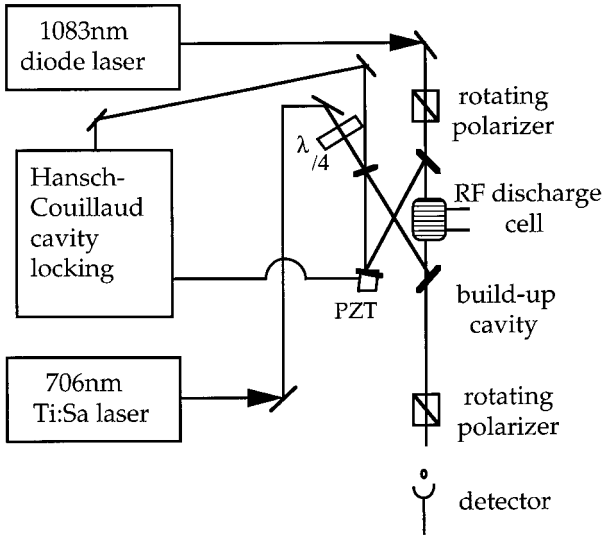


**Fig. 2.** Experimental apparatus.

$2P_1 \leftrightarrow 3S_1$ transitions, respectively, with a Rabi frequency $\Omega_L$ exceeding the typical values for power and collisional broadening of the transitions in the discharge regime. Under these circumstances two-photon absorption across the (long) $2S_1 \leftrightarrow 3S_1$ transition is substantially smaller than the two single-photon absorption over the $2S_1 \leftrightarrow 2P_1$ and $2P_1 \leftrightarrow 3S_1$ channels [17] or [20]. Owing to Zeeman degeneracy the transparency of the probe beam involves more than one three-level configuration the couples the magnetic sub-levels of the $2S_1$, $2P_1$ and $3S_1$ states.

The prototype atomic system is comprised of three sets of states (*cf.* Fig. 1a): the lower and upper levels $|\,{\rm c}\rangle$ and $|\,{\rm b}\rangle$ are coupled by electric-dipole transitions to the common intermediate level $|\,{\rm a}\rangle$. The strong coupling laser AC Stark shifts some levels of the upper doublet resulting into a pair of dressed states. The dressed-atom hamiltonian takes the form [18]

$$\begin{aligned} H =& \hbar\,\omega_{\rm L}\left(a_{\rm L}^{\dagger}a_{\rm L}+\frac{1}{2}\right)\hbar\,\omega_0\,|\,{\rm b}\rangle\langle\,{\rm b}\,| \\ &+(\hbar\,g_{\rm L}\,|\,{\rm a}\rangle\langle\,{\rm b}\,|\,a_{\rm L}^{\dagger}+H.C.) \end{aligned} \tag{1}$$

where $\hbar\ g_{\rm L} = \langle\,{\rm a}\mid\hat{\mathbf{d}}\mid\,{\rm b}\,\rangle\cdot\boldsymbol{\varepsilon}_{\rm L}\sqrt{\hbar\,\omega_{\rm L}/2\varepsilon_0 V}$ with a standard notation for the parameters. Dressed states for the $N$-manifold and a positive detuning $\delta_{\rm L}$ (*cf.* Fig. 1b)

$$|\,1(N)\rangle = \sin\ \theta_N\,|\,{\rm a};\ N+1\rangle + \cos\ \theta_N\,|\,{\rm b};\ N\rangle$$

and

$$|\,2(N)\rangle = \cos\ \theta_N\,|\,{\rm a};\ N+1\rangle + \sin\ \theta_N\,|\,{\rm b};\ N\rangle, \tag{2}$$

with coefficients given by

$$\sin\ 2\theta_N = \frac{\Omega_{\rm L}(N)}{\Omega_{\rm R}(N)} \quad \text{and} \quad \cos\ 2\theta_N = \frac{-\delta_{\rm L}}{\Omega_{\rm R}(N)} \tag{3}$$

are eigenstates of (1) with the following eigenvalues

$$E_{1N} = \hbar \left[ \omega_{\rm L}(N+1) - \frac{\delta_{\rm L}}{2} + \frac{\Omega_{\rm R}}{2} \right]$$

and

$$E_{2N} = \hbar \left[ \omega_{\rm L}(N+1) - \frac{\delta_{\rm L}}{2} - \frac{\Omega_{\rm R}}{2} \right]. \qquad (4)$$

Here $N$ is the number of photons of the coupling laser while $\Omega_{\rm L}(N) = 2|g_{\rm L}|^2\sqrt{N+1}$ is the *Rabi frequency* and $\Omega_{\rm R}(N) = \sqrt{\delta_{\rm L} + \Omega_{\rm L}(N)}$ the *generalized Rabi frequency.* It is clear that at resonance ($\theta_N = \pi/4$) the intermediate level $2P_1$ affects with equal probability either dressed states so that absorption of probe beam photons takes place along both paths $|\ {\rm c};\ N+1\rangle \rightarrow |\ 1(N)\rangle$ and $|\,{\rm c}\ ;\ N+1\rangle \rightarrow |\,2(N)\rangle$. The corresponding transition amplitudes $\langle {\rm c};\ N+1\,|\,\hat{\mathbf{r}}\cdot\boldsymbol{\varepsilon}_{\rm pr}\,|\,1(N)\rangle$ and $\langle {\rm c};\ N+1\,|\,\hat{\mathbf{r}}\cdot\boldsymbol{\varepsilon}_{\rm pr}\,|\,2(N)\rangle$ can be evaluated with the help of equation (2) and the probe absorption rate, including the contribution from the absorption to the unperturbed level ($M_{\rm J} = 0$) of the $2P_1$ state, can be written in the form

$$r_{\rm abs} = k\sin^2\alpha + k'(1+\cos^2\alpha) \qquad (0 < k' < k) \qquad (5)$$

where $\alpha$ denotes the angle between the polarization $\varepsilon_{\rm pr}$ of the probe and the polarization $\varepsilon_{\rm L}$ of coupling laser. The first term in (5) originates from the absorption to the unperturbed level while the other represents absorption to the levels $E_{1N}$ and $E_{2N}$. Here $k$ depends on the frequency separation and reduced matrix element of the transition to which the probe is coupled while $k'$ depends, in addition, on the Rabi frequency $\Omega_{\rm L}$; $k' \rightarrow k$ in the absence of the coupling laser but it reduces to zero when the coupling laser becomes so intense that the probe progressively falls outside the overlap between the widths of the two AC Stark shifted levels. The unperturbed rate $r^0_{\rm abs}$ (coupling laser off) is equal to $2k$; we find instructive to isolate in $r^0_{\rm abs}$ the unperturbed level absorption term as it appears in equation (5), *i.e.*,

$$r^0_{\rm abs} = k\ \sin^2\alpha + k(1+\cos^2\alpha) \qquad (6)$$

so that comparison with equation (5) shows dropping of the absorption rate $r_{\rm abs}$ below $r^0_{\rm abs}(k' < k)$ when the coupling laser is on. The expected dependence of the probe absorption and its contrast,

$$c = 1 - \frac{r_{\rm abs}}{r^0_{\rm abs}} = \frac{1+\cos^2\alpha}{2}\left(1 - \frac{k'}{k}\right), \qquad (7)$$

on $\alpha$ has been experimentally verified as shown in Figure 3. In the absence of coupling laser (Eqs. (5, 6)) coincide yielding a vanishing contrast and no induced transparency while complete transparency corresponds to a contrast equal to unity which is expected to occur for parallel polarized beams and laser intensities $I_{\rm L}$ high enough to render the probe only loosely coupled to the perturbed levels.

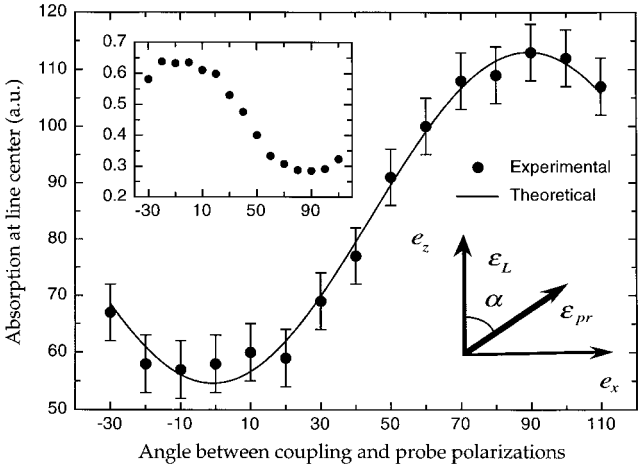


**Fig. 3.** Absorption profile of the probe laser beam *vs.* the angle between the polarizations of the coupling ($\varepsilon_{\rm L}$) and probe ($\varepsilon_{\rm pr}$) beams. The polarization $\varepsilon_{\rm L}$ is fixed along $\mathbf{e}_z$ (quantization axis) while $\varepsilon_{\rm pr}$ sweeps different angles $\alpha$ in the plane $\mathbf{e}_x - \mathbf{e}_z$. The two beams, counter propagating along $\mathbf{e}_y$, are resonant with the $2S_1 \rightarrow 2P_1$ and $2P_1 \rightarrow 3S_1$ transitions, respectively. Probe beam absorption contrast (Inset).

The intense laser that couples the levels $|\,{\rm a}\rangle$ and $|\,{\rm b}\rangle$ splits the probe absorption line into two components each centered at the transition frequencies from $|\ 1(N)\rangle$ and $|\,2(N)\rangle$ to the lower level $|\,{\rm c}\rangle$. These two components are separated by the Autler-Townes splitting given by the difference $(E_{1N} - E_{2N})$ in equation (4). The experimental results of Figure 4 exhibits the presumed dependence of the splitting as a function of (a) detuning $\delta_{\rm L}$ (fixed power) and as a function of (b) the power (fixed detuning).

The linewidth of the transmitted probe signal is determined by the linewidth of the Autler-Townes sidebands each given by the sum of the width of the level $|\,{\rm c},\ N+1\rangle$ and the width of the level $|\ 1(N)\rangle$ or $|\ 2(N)\rangle$. Figure 5a shows the absorption profile of the probe beam when this is scanned through the $2S_1 \rightarrow 2P_0$ transition in the absence of the coupling laser: it consists of a Doppler broadened Gaussians with a linewidth of 2 GHz. The probe absorption exhibits instead a dip when the coupling laser, resonant with the $2P_0 \rightarrow 3S_1$ transition, is switched on and held fixed at the center of the Gaussian profile as the probe is scanned across the entire line profile. In our case the Rabi frequency $\Omega_L$ of the coupling laser largely exceeds the levels linewidth. The appropriate (ladder) scheme for the relevant levels is shown in Figure 5b. The slight growth of the absorption in proximity of the two Autler-Townes peaks is associated with transitions from the common ground $|\ {\rm c},\ N+1\rangle$ to the dressed $|\ 1(N)\rangle$ and $|\,2(N)\rangle$ levels; but one would expect the absorption to be somewhat the same as in the unperturbed case when the probe is swept away from the peaks area as observed, *e.g.*, outside the peaks. Conversely, across the two Autler-Townes peaks, where the probe is effectively coupled to neither ones of the dressed levels for separations sufficiently larger than the level broadenings, we observe a

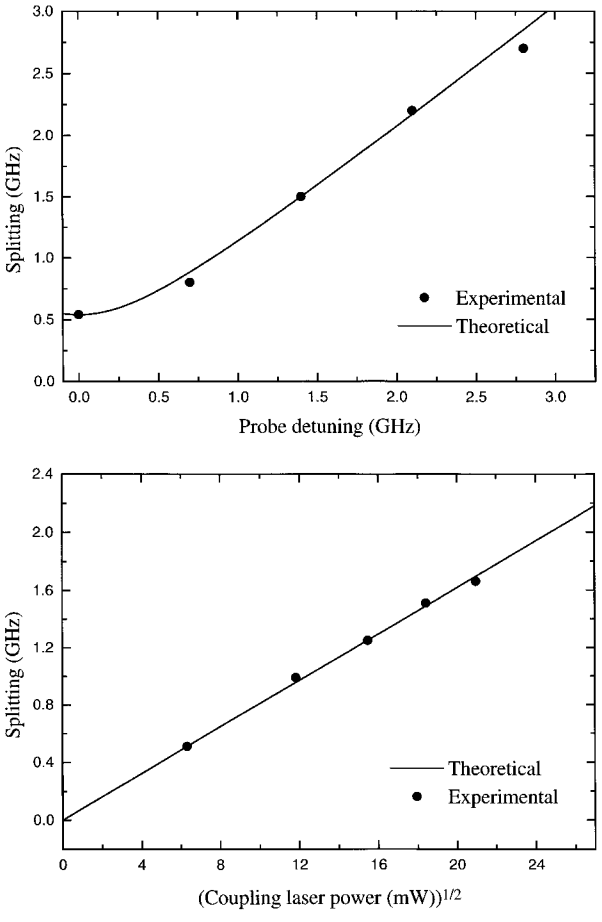


**Fig. 4.** Autler-Townes splitting *vs.* (a) the detuning $\delta_{\rm L}$ of the coupling laser ($10^3$ W/cm$^2$) and *vs.* (b) the square root of the power ($\delta_{\rm L} = 0$). The probe and coupling laser beams, with parallel polarizations, are coupled to the $2S_1 \rightarrow 2P_1$ and $2P_1 \rightarrow 3S_1$ transitions. The gas pressure in the cell is 30 mTorr.

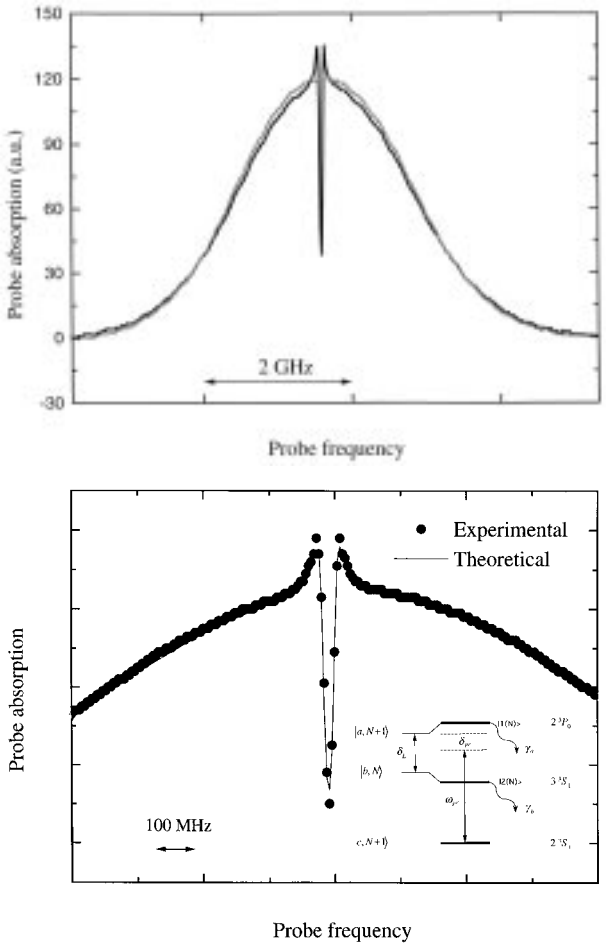


**Fig. 5.** (a) Absorption profile (black curve) showing induced transparency of the probe beam (1.7 mW/cm$^2$) scanned through the $2S_1 \rightarrow 2P_0$ transition when the coupling laser (10 W/cm$^2$) is kept tuned onto resonance with the $2P_0 \rightarrow 3S_1$ transition. Absorption Gaussian profile (grey curve) of the probe beam when the coupling laser is off. Both beams have linear polarizations parallel to $\mathbf{e}_z$. (b) Blow-up of the transparency window dip with fitting provided by the theory with parameters $KI_{\rm L} = 4$ and $\gamma_{\rm a} \cong \gamma_{\rm b} = 15$ MHz and scheme of the relevant levels (inset). The helium pressure is kept constant at 120 mTorr.

large transparency window. This can arise from interfering processes that coherently couple $|\,1(N)\rangle$ and $|\,2(N)\rangle$ through the common lower level $|\,{\rm c},\ N+1\rangle$ with no net absorption of probe photons. This explanation has been put forward, *e.g.*, in [16]. Although the lineshapes that we observe could be discussed within the dressed states framework, as anticipated above, in the following we will adopt a straightforward approach by considering a nonlinear susceptibility for a three-level configuration of the form [17,19]

$$\chi_{\rm pr} = -\frac{N\,|\mu_{\rm ca}|^2}{\hbar} \times \frac{(\delta_{\rm pr}+\delta_{\rm L}-i\gamma_{\rm b})}{(\delta_{\rm pr}-i\gamma_{\rm a})(\delta_{\rm pr}+\delta_{\rm L}-i\gamma_{\rm b})-\gamma_{\rm a}\gamma_{\rm b}KI_{\rm L}}\,. \qquad (8)$$

We denote by $\delta_{\rm L}$ and $\delta_{\rm pr}$ the detunings of the two laser beams, $I_{\rm L}$ the intensity of the coupling laser, $\mu_{\rm ca}$ the matrix element relevant to the $|\,{\rm a},\ N+1\rangle \rightarrow |\,{\rm c},\ N+1\rangle$ transition and $N$ is the atomic density. The factor $K$ depends on the saturation intensity of the coupling laser ($I_{\rm L}^{\rm sat}$) as well as on the linewidths $\gamma_{\rm a}$ and $\gamma_{\rm b}$ of the $2S_1 \rightarrow 2P_0$ and $2P_0 \rightarrow 3S_1$ transitions. At the pressures, the densities and the rather large fields needed to maintain the discharge collisional and power broadening are the dominant contributions to the widths of the resonances so that $\gamma_{\rm a}$ and $\gamma_{\rm b}$ appear in equation (8) as effective linewidths accounting for both effects. It is seen from equation (8) that when the parameter $KI_{\rm L}$ becomes larger than unity, then control of the probe absorption is possible and a significant amount of induced transparency can be achieved. This condition implies that the intensity ($I_{\rm L}$) of the coupling laser becomes appreciably larger than the saturation intensity $I_{\rm L}^{\rm sat}$ times the ratio of the effective linewidths $\gamma_{\rm a}$ and $\gamma_{\rm b}$ . When this condition is released, on the other hand, the mechanism of electromagnetically induced transparency starts to degrade and other absorption channels, *e.g.*, two-photon

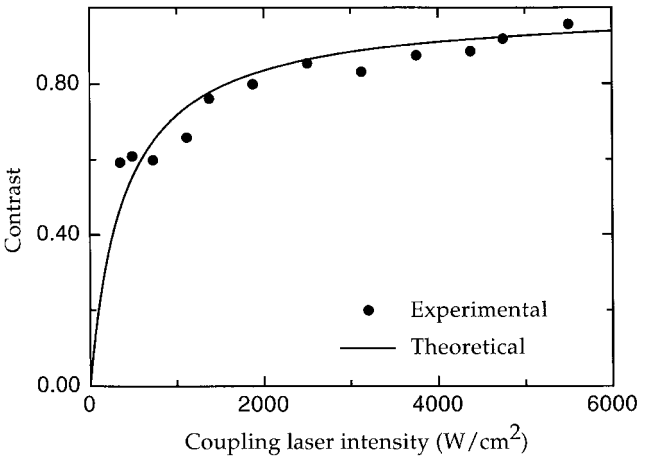


**Fig. 6.** Contrast of the probe absorption dip *vs.* the coupling laser intensity and theoretical fitting with $K = 140$ cm$^2$/W (solid line). Experimental conditions are same as in Figure 5.

absorption also begin to play an important role [20]. Probe absorption is given by the imaginary part of susceptibility in (8): this, when properly averaged over a Maxwell distribution of velocities to account for the Doppler effect, reproduces the transparency profile of Figure 5a for a value of $KI_{\rm L}$ close to 4 and effective linewidths $\gamma_{\rm a} \cong \gamma_{\rm b}$ of 15 MH$z$. These values of the linewidth have been estimated from standard measurements of saturation spectroscopy (Lamb dip recording with counter propagating laser beams) on the $2S_1 \rightarrow 2P_0$ and $2P_0 \rightarrow 3S_1$ transition with a probe power $2 \times 10^2$ $\mu$W/mm$^2$ at a He pressure 120 mTorr. The lineshape profile originates from the envelope of absorptions of all velocity classes weighted by the relevant Maxwell distribution. For a zero-velocity class the resonant coupling laser produces a symmetric Autler-Townes splitting while for any other class of velocities the splitting is asymmetric. For suitable high powers of the coupling laser the splitting profiles exhibit low absorptions on the resonant central frequency for counter propagating probe and coupling beams so that the transparency contrast is independent on the Doppler width. Although a more adequate explanation should include effects of population and level degeneracy agreement with this experimental result is quite satisfactory as shown by the solid line in Figure 5b.

Figure 6 shows the behavior of the contrast of the absorption dip as the intensity of the coupling laser is varied. The contrast defines deviations from unit of the ratio between the center-line probe absorption and the center-line absorption of the unperturbed Gaussian. When the two laser beams are resonant, the probe absorption for a sufficiently intense coupling laser is given by the imaginary part $\tilde{\chi}$ of the susceptibility in equation (8) as

$$\tilde{\chi}_{\rm pr} \cong -\frac{N\,|\mu_{\rm ca}|^2}{\hbar}\frac{1}{\gamma_{\rm a}(1+KI_{\rm L})} \qquad (9)$$

and likewise the unperturbed absorption is

$$\tilde{\chi}^0_{\rm pr} \cong -\frac{N\,|\mu_{\rm ca}|^2}{\hbar}\frac{1}{\gamma_{\rm a}}\,. \qquad (10)$$

For a sufficiently intense coupling beam the probe absorption and contrast vary with the inverse of the intensity $I_{\rm L}$ which conform to our experimental result. Nearly full bleaching is observed for intensities above 5000 W/cm$^2$ that corresponds to values of $KI_{\rm L} \geq 10$. The parameter $KI_{\rm L}$ seems to play an important role in controlling the induced transparency in a helium discharge. Generally speaking, when the Rabi frequency of the coupling laser substantially exceeds the square root of the product of the effective linewidths $\gamma_{\rm a}$ and $\gamma_{\rm b}$ the medium becomes transparent to the probe which is otherwise absorbed.

We have also analized the behaviour of the probe contrast as the pressure gas in the discharge is varied. To a certain extent increasing values of the pressure lead to a linear increase in the number of metastable atoms. In a discharge, however, the processes of metastabilization due, *e.g.*, to the electron- atoms and ions-atoms collisions definitely restrain the growth of metastable atoms with increasing gas pressures. Owing to this a maximum in the density metastable atoms should then be reached and followed by lower densities as the pressure is further increased. Because the effective linewidth is proportional to the average number of metastable atoms it is fairly reasonable to assume that in our case the $\gamma$'s vary with pressure ($p$) according to the same dependence which we take of the form

$$\gamma(p) = ap + bp^2cp^{-1} + cp^{-2} \qquad (a, b, c, d \quad \text{coefficients}). \qquad (11)$$

With the help of the ansatz (Eq. (11)) we have derived an expression for the contrast as a function of the pressure by substituting $\gamma_{\rm a}(p) \cong \gamma_{\rm b}(p)$ in equation (8) to fit the experimental data of Figure 7 with the available coefficients. The somewhat satisfactory agreement seems to indicate that slightly higher transparencies occur at pressures that correspond to an optimal metastabilization rate. Also, the high pressures used in the cell increase collisional broadening of the transitions which justifies the quite large power densities of the laser beams required to reach induced transparency.

Owing to the intrinsic Zeeman degeneracy of the atomic structure of helium we have dealt so far with induced transparency involving three-level patterns that couple different magnetic sub-levels. There are choices of the laser polarization which enable to select a unique path $2S_1 \leftrightarrow 2P \leftrightarrow 3S_1$. The observation of different paths could be obtained by removing the Zeeman degeneracy with a magnetic field. The probe absorption, *e.g.*, on the $2S_1(M = 1) \leftrightarrow 2P_1(M = 0) \leftrightarrow 3S_1(M = +1)$ path occurs at a lower frequency than that for the other channel $2S_1(M = -1) \leftrightarrow 2P_1(M = 0) \leftrightarrow 3S_1(M = +1)$. The set of results in Figure 8 show the induced transparencies recorded by chopping the coupling laser in the presence

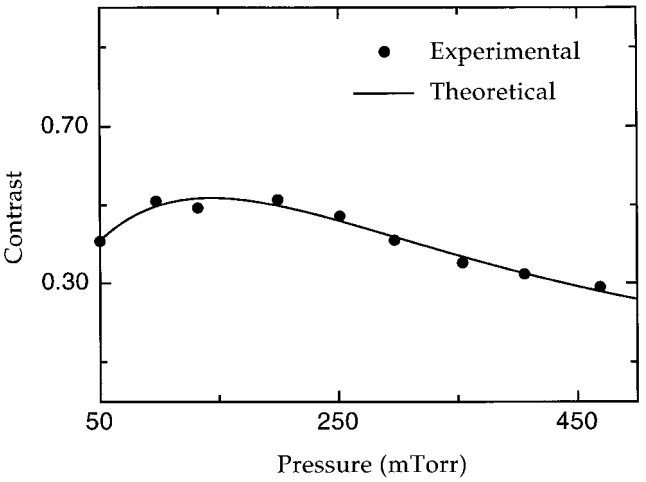


**Fig. 7.** Contrast profile showing probe beam induced transparency *vs.* the pressure of the gas discharge in the cell and fitting from the theory (solid line). The two beams with parallel linear polarizations have power densities 6 W/cm$^2$ and 2.5 kW/cm$^2$ and are coupled, respectively, to the transition $2S_1 \rightarrow 2P_1$ and $2P_1 \rightarrow 3S_1$.

of a magnetic field. Only the transparency dips are shown since the Gaussian profile is removed by synchronous lock-in detection. Figure 8a refers to the case in which probe and coupling lasers have parallel linear polarizations and perpendicular to the magnetic field: in this case there appear four transition paths which correspond to the decomposition of the two linear polarizations in all possible combinations of circular ones. Figure 8b shows instead the transparency characteristics of selected paths obtained by setting a left handed polarized probe and a left handed polarized coupling laser. In this case only a single path is selected as we illustrate in the inset.

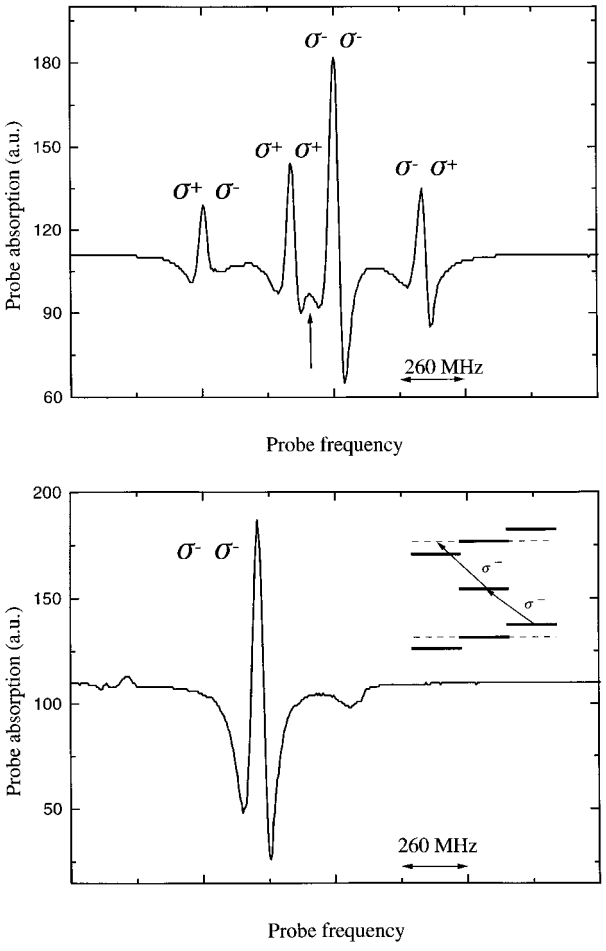


**Fig. 8.** Probe beam (30 mW/cm$^2$) absorption dip *vs.* detuning in the presence of a magnetic field of 75 Gauss: (a) both beams parallel linearly polarized and perpendicular to the magnetic field, (b) probe and coupling beams left handed polarized. The inset shows the individual three-level pattern with which induced transparency is achieved. The coupling beam (300 W/cm$^2$) is tuned onto resonance with the $2P_0 \rightarrow 3S_1$ transition. The gas pressure is 200 mTorr.

## Conclusions

We have extended the observation of electromagnetically induced transparency to a radio-frequency discharge of metastable $^4$He. Total bleaching of a weak probe laser beam has been obtained in spite of the heavy collisional processes and intense laser fields that can easily degrade the atomic level coherence that is essential for the demonstration of electromagnetically induced transparency. The effect of gas pressure on the transparency has been investigated and we found that higher values of transparency seem to occur at pressures corresponding to an optimal metastabilization rate. Large values of induced transparency are observed for intense non resonant excitations of the Autler-Townes levels and the level separation becomes sufficiently larger than the power and collisional broadenings of the relevant transitions. This suggests [16] the presence of interference between processes that coherently couple the dressed levels *via* a common lower level with no net absorption of probe photons. The dependence of electromagnetically induced transparency on the relative polarizations of the coupling and probe beams has further permitted to demonstrate how transparency varies when one or more paths (Zeeman level degeneracy) contribute to the probe absorption process. Similar results have been obtained by removing the degeneracy through the application of an external magnetic field. Because of the diverse combinations accessible electromagnetically induced transparency in a discharge opens interesting perspectives. Moreover, the use of an intermediate level radiatively connected to a lower level could lead to light induced transparency at wavelengths much shorter than that of the dressing laser, providing a novel tool for the manipulation of coherent radiation. Under particular discharge conditions, we believe that gain without inversion on the probe could also be obtained, opening the prospect of lasing without inversion in the X-UV regime.

We are particularly indebted to Dr. A. Bambini for enlightening discussions and suggestions. We are thankful to the I.N.F.M. and the European Union (contract ♯ GE1*CT920046 and ERB FMGE CT950017) for financial support.

## References

1. K.J. Boller, A. Imamoglu, S.E. Harris, Phys. Rev. Lett. **66**, 2593 (1991).
2. P. Lambropoulos, P. Zoller, Phys. Rev. **24**, 379, (1981).
3. K. Rzazewski, J. Eberly, Phys. Rev. Lett. **47**, 408 (1981).
4. S. Ravi, G.S. Agarwal, Phys. Rev. A **35**, 3354 (1987).
5. R. Whitley, C. Stroud, Phys. Rev. A **14**, 1498, (1976).
6. G. Alzetta, A. Gozzini, L. Moi, G. Orriols, Nuovo Cimento **36B**, 5 (1976).
7. G. Grynberg, M. Pinard, P. Mandel, Phys. Rev. A 54, 776 (1996); C. Fort, F.S. Cataliotti, T.W. Hänsch, M. Inguscio, M. Prevedelli, Opt. Comm. **139**, 31 (1997).
8. See, *e.g.*, O. Kocharovskaya, P. Mandel, Quantum Opt. **6**, 217 (1994); A.S. Zibrov, M.D. Luckin, D.E. Nikonov, L. Hollberg, M.O. Scully, V.L. Velichansky, H.G. Robinson, Phys. Rev. Lett. **75**, 1499 (1995).
9. K. Hakuta, L. Marmet, B.P. Stoicheff, Phys. Rev. A **45**, 5152 (1992); S.E. Harris, J.E. Field, A. Imamoglu, Phys. Rev. Lett. **64**, 1107 (1990).
10. A. Aspect. E. Arimondo, R. Kaiser, N. Vansteerkiste, C. C- Tannouudji, Phys. Rev. Lett **61**, 826 (1988); C. Fort, F.S. Cataliotti, M. Prevedelli, M. Inguscio, Opt. Lett. **22**, 1107 (1997).
11. S.E. Harris, Optics Lett. **19**, 2018, (1994).
12. P.L. Knight, M.A. Lauder, and B.J. Dalton, Phys. Rep. **190**, 1 (1990).
13. D. Fulton, S. Shepherd, R.R. Moseley, B.D. Sinclair, M.H. Dunn, Phys. Rev A **52**, 2302 (1995).
14. F.S. Pavone, G. Bianchini, F.S. Cataliotti, T.W. Hänsch, M. Inguscio, Optics Lett. **22**, 736 (1997).
15. A. Kasapi, Phys. Rev. Lett. **77**, 1035 (1996).
16. J. Field, K. Hahn, S. Harris, Phys. Rev. Lett. **67**, 3062 (1991).
17. S. Scandolo, F. Bassani, Phys. Rev. B **45**, 13 257 (1992).
18. C. Cohen-Tannouudji, J. Dupont-Roc, G. Grynberg in Atom-Photon Interactions (J. Wiley & Sons, Inc. 1992).
19. T.W. Hänsch, Z. Phys. **236**, 213 (1970).
20. D. Ricca, F. Bassani, Nuovo Cimento **20**, 801 (1983).